

Monopoles in AdS

Paul Sutcliffe

Department of Mathematical Sciences, Durham University, Durham DH1 3LE, U.K.

Email: p.m.sutcliffe@durham.ac.uk

April 2011

Abstract

Applications to holographic theories have led to some recent interest in magnetic monopoles in four-dimensional Anti-de Sitter spacetime. This paper is concerned with a study of these monopoles, using both analytic and numerical methods. An approximation is introduced in which the fields of a charge N monopole are explicitly given in terms of a degree N rational map. Within this approximation, it is shown that the minimal energy monopole of charge N has the same symmetry as the minimal energy Skyrmion with baryon number N in Minkowski spacetime. Beyond charge two the minimal energy monopole has only a discrete symmetry, which is often Platonic. The rational map approximation provides an upper bound on the monopole energy and may be viewed as a smooth non-abelian refinement of the magnetic bag approximation, to which it reverts under some additional approximations. The analytic results are supported by numerical solutions obtained from simulations of the non-abelian field theory. A similar analysis is performed on the monopole wall that emerges in the large N limit, to reveal a hexagonal lattice as the minimal energy architecture.

1 Introduction

The AdS/CFT correspondence allows the investigation of strongly coupled theories by studying classical solutions in the bulk. Recently, it has been argued that interesting phenomena may result, including spontaneous breaking of translational symmetry, if the bulk Anti-de Sitter (AdS) spacetime contains non-abelian magnetic monopoles [1]. This provides motivation for a detailed study of $SU(2)$ magnetic monopoles in four-dimensional AdS spacetime.

In addition to holographic applications, there are other reasons to consider monopoles in AdS. In Minkowski spacetime, when the Higgs field is massless, there is a $4N$ -dimensional moduli space \mathcal{M}_N of static charge N BPS monopoles. In contrast, the attraction in AdS spacetime should produce a unique minimal energy monopole for each charge N (up to the obvious action of spatial rotations). It is of interest to determine the structure and symmetry of the N -monopole, which will map to a unique point in the moduli space \mathcal{M}_N as the AdS curvature tends to zero.

It has been known for some time that there are many similarities between BPS magnetic monopoles and Skyrmions (for a review see [2]). However, one important difference is the attractive force between Skyrmions, producing bound states, in contrast to the BPS monopole moduli space \mathcal{M}_N , resulting from the absence of static forces between monopoles. It is therefore expected that studying monopoles in AdS will enhance the similarities with Skyrmions, since both will share the features of attractive forces and bound states.

Motivated by previous work on Skyrmions [3], an approximation is introduced in which the non-abelian fields of an N -monopole in AdS are written in terms of a degree N rational map between Riemann spheres. The Yang-Mills-Higgs energy functional leads to an energy functional on the space of rational maps, which is precisely the one found in the similar approach to Skyrmions. This implies that, within this approximation, the minimal energy monopole of charge N in AdS has the same rotational symmetry group as the minimal energy Skyrmion with baryon number N and massless pions in Minkowski spacetime.

In particular, this approach predicts that the 1-monopole is spherically symmetric and the 2-monopole is axially symmetric, but for charges greater than two the minimal energy monopole has only a discrete symmetry group, which is often Platonic.

In Minkowski spacetime the existence of particular BPS monopole solutions with Platonic symmetries has been proved [4, 5] using the Nahm transform [6], but in the BPS case there is no energetic preference for these solutions, because of the democracy of the moduli space \mathcal{M}_N . Although the rational map approximation does not produce any exact solutions, beyond charge one, it does provide an upper bound on the N -monopole energy and suggests that in moving from Minkowski spacetime to AdS, the breaking of the energy degeneracy of the moduli space \mathcal{M}_N leaves particular symmetric monopoles as the minimal energy solutions.

Monopoles with large charge have been considered previously using the magnetic bag approximation, both in Minkowski spacetime [7] and in AdS [1]. The magnetic bag approximation assumes that inside a spherical bag both the Higgs field and the magnetic field vanish and outside the bag there is an abelian magnetic field. The rational map approximation may

be viewed as a smooth non-abelian refinement of the magnetic bag approximation, to which it reverts under some additional approximations.

Simulations of the full non-abelian field theory are performed to provide numerical solutions for monopoles in AdS, with charges from 1 to 17. These numerical results provide support for both the approximate analytic treatment using rational maps, and the magnetic bag approximation. The numerical results also reveal interesting information about the zeros of the Higgs field. For most of the solutions, there is a zero of the Higgs field with multiplicity N located at the origin. However, for $N = 3$ and some further non-minimal solutions with higher charge, there are $N + 2$ zeros of the Higgs field, with one of the zeros having a negative multiplicity.

By zooming to the Poincaré patch in the large N limit, the study of magnetic monopoles translates into the investigation of monopole walls in AdS. A monopole wall [8] is a novel domain wall in which the magnetic field along a line perpendicular to the wall tends to zero on one side of the wall and to a non-zero constant on the other side of the wall. The fields are periodic in the directions parallel to the wall, with a non-trivial spatial variation of the energy density and magnetic field. Monopole walls have infinite energy per unit area in Minkowski spacetime, but in AdS this is finite and they can be studied using a magnetic bag style approximation [1].

The magnetic bag approximation is too crude to reveal any information concerning the spatial distribution of the fields parallel to the wall, but a variant of the rational map approximation, involving elliptic functions, is refined enough for this purpose. It suggests that the minimal energy per unit area is obtained from a monopole wall with a hexagonal lattice. Numerical simulations are performed that support this conclusion, which is again in agreement with the Skyrme model, where a similar hexagonal lattice exists [9].

Previous studies of monopoles in AdS have been restricted to the spherically symmetric single monopole [10, 11], and axially symmetric monopoles with charges two and three [12]. The computations in [12] reveal that the energy of the charge two monopole is greater than twice the energy of the single monopole, but this result was incorrectly interpreted to conclude that monopoles repel and that the axially symmetric 2-monopole is unstable. The source of the confusion is that in Minkowski spacetime the following argument can be applied: if the energy of an N -soliton is greater than N times the energy of a single soliton, then the energy of the N -soliton can be reduced by infinitely separating the N constituents. However, in AdS this argument fails because the energy of a single soliton increases as it approaches the boundary of AdS. The energy of the single soliton, which is used in the false comparison, is the single soliton energy only when the soliton is located at the origin of AdS. At first glance this may appear confusing, given the large isometry group, $O(3, 2)$ of AdS, but there is an important subtlety at work here. To consider static solutions, and their associated energies, requires the selection of a time-like Killing vector. This breaks the isometries of AdS and introduces a preferred point in space, which is denoted the origin. Solitons are attracted towards the origin, which is consistent with the interpretation of AdS as gravitational attraction.

2 Monopoles, rational maps and magnetic bags

In terms of sausage coordinates, the metric of four-dimensional AdS spacetime may be written as

$$ds^2 = -\left(\frac{1+\rho^2}{1-\rho^2}\right)^2 dt^2 + \frac{4L^2}{(1-\rho^2)^2} \left(d\rho^2 + \rho^2(d\theta^2 + \sin^2\theta d\varphi^2)\right), \quad (2.1)$$

where the range of the radial coordinate is $0 \leq \rho \leq 1$ and L is the AdS radius, related to the cosmological constant via $\Lambda = -3/L^2$. The above choice of coordinates for AdS is motivated by later numerical investigations, as it is more efficient to have a finite range for the coordinates.

The Yang-Mills-Higgs action is

$$S = \int \frac{1}{2} \text{Tr} \left(\frac{1}{4} F_{\mu\nu} F^{\mu\nu} + \frac{1}{2} D_\mu \Phi D^\mu \Phi \right) \sqrt{-g} d^4x, \quad (2.2)$$

where the gauge potential A_μ and Higgs field Φ are both $su(2)$ -valued. The massless Higgs field transforms in the adjoint representation of $SU(2)$ and is subject to the boundary condition $|\Phi|^2 = -\frac{1}{2} \text{Tr} \Phi^2 \rightarrow 1$ as $\rho \rightarrow 1$.

At a fixed time, the Higgs field on the spatial boundary is a map between two spheres, $\Phi|_{\rho=1} : S^2 \mapsto S^2$, with winding number $N \in \pi_2(S^2) = \mathbb{Z}$. This winding number is equal to the magnetic charge of the monopole, in units of 2π , and may also be written as the integral

$$N = \frac{1}{4\pi} \int \varepsilon_{ijk} \text{Tr}(F_{jk} D_i \Phi) d^3x. \quad (2.3)$$

Static monopoles are critical points of the static energy associated with the action (2.2), namely

$$E = - \int \frac{1}{2} \text{Tr} \left(\frac{1}{4} F_{ij} F^{ij} + \frac{1}{2} D_i \Phi D^i \Phi \right) \sqrt{-g} d^3x. \quad (2.4)$$

The aim is to find the global minimum of this energy, within each topological sector given by the positive integer N . Note that the above normalizations are such that in Minkowski spacetime each point of the BPS moduli space \mathcal{M}_N is associated with a monopole solution with energy $2\pi N$.

It is perhaps worth pointing out that although constant time slices of the metric (2.1) give the Poincaré ball model of hyperbolic space, the static energy (2.4), and hence the static field equation, is not the much studied system for monopoles in hyperbolic space [13]. This is because of the extra factor $\sqrt{-g_{tt}} = (1+\rho^2)/(1-\rho^2)$ hidden in the term $\sqrt{-g}$ from the warp factor in the metric (2.1).

In Minkowski spacetime there is a diffeomorphism, preserving the action of spatial rotations, between the BPS moduli space \mathcal{M}_N and a certain equivalence class of degree N rational maps between Riemann spheres [14]. The rational map appears as scattering data along a radial half-line of an operator constructed from the monopole fields. As the inverse

scattering problem is not tractable for $N > 1$, there is no explicit formula for the monopole fields in terms of the rational map.

Motivated by similarities between monopoles and Skyrmons, an explicit but approximate description of Skyrmons was introduced in terms of rational maps [3]. Continuing the theme of an interplay between monopoles and Skyrmons, the rational map approximation for Skyrmons will now be adapted back to the monopole context, to provide approximate fields for monopoles in AdS.

A rational map between Riemann spheres, $R(z)$, is simply a ratio of two polynomials in a complex variable z . The two polynomials are required to have no common roots, and the degree of the rational map is the largest of the degrees of the two polynomials. To make the connection to monopoles (or Skyrmons) the Riemann sphere coordinate z is related to the angular space coordinates θ and φ via standard stereographic projection, that is $z = e^{i\varphi} \tan(\theta/2)$.

The Riemann sphere coordinate, R , on the target space of the rational map, is related to a three-component unit vector \mathbf{n} by inverse stereographic projection,

$$\mathbf{n} = \frac{1}{1 + |R|^2} (R + \bar{R}, i(\bar{R} - R), 1 - |R|^2). \quad (2.5)$$

The approximate monopole fields in AdS are taken to be

$$\Phi = iH\mathbf{n} \cdot \boldsymbol{\tau}, \quad A_j = \frac{i}{2}(1 - K)(\mathbf{n} \times \partial_j \mathbf{n}) \cdot \boldsymbol{\tau}, \quad (2.6)$$

where $H(\rho)$ and $K(\rho)$ are real radial profile functions. Regularity at the origin imposes the boundary conditions $H(0) = 0$ and $K(0) = 1$. The conditions at the spatial boundary of AdS follow from the requirement that as $\rho \rightarrow 1$ then $|\Phi| \rightarrow 1$ and $D_j \Phi \rightarrow 0$. This provides the boundary conditions $H(1) = 1$ and $K(1) = 0$.

A more general form for the gauge potential, using all the symmetric tensors that can be computed from \mathbf{n} , appears to be

$$A_j = \frac{i}{2}(1 - K)(\mathbf{n} \times \partial_j \mathbf{n}) \cdot \boldsymbol{\tau} + \frac{i}{2}P \partial_j \mathbf{n} \cdot \boldsymbol{\tau} + \frac{i}{2}Q \hat{x}_j \mathbf{n} \cdot \boldsymbol{\tau}, \quad (2.7)$$

with additional profile functions $P(\rho)$ and $Q(\rho)$. However, Q corresponds to an abelian gauge potential in the reduced one-dimensional radial theory, and therefore may be set to zero by a gauge transformation. Furthermore, there is a global $U(1)$ symmetry that rotates the fields K and P , and this can be used to set P to zero.

As $\Phi|_{\rho=1} = i\mathbf{n} \cdot \boldsymbol{\tau}$, it is obvious that the monopole charge N , which is the winding number of the Higgs field on the boundary two-sphere, is equal to the degree of the rational map $R(z)$ that determines \mathbf{n} via (2.5). It will be useful later to note the integral expression for the degree

$$N = \frac{1}{4\pi} \int \left(\frac{1 + |z|^2}{1 + |R|^2} \left| \frac{dR}{dz} \right| \right)^2 \frac{2i dz d\bar{z}}{(1 + |z|^2)^2} \quad (2.8)$$

where the final factor in (2.8) is simply the standard area element on the two-sphere.

Substituting the approximate fields (2.6) into the energy (2.4) yields the expression

$$E^{rat} = 4\pi L \int_0^1 \left\{ \frac{1}{(1-\rho^2)^2} (\rho^2 H'^2 + 2NH^2 K^2) + \frac{1}{16L^2} \left(2NK'^2 + \frac{\mathcal{I}}{\rho^2} (K^2 - 1)^2 \right) \right\} (1 + \rho^2) d\rho, \quad (2.9)$$

where \mathcal{I} is defined as the following energy functional on the space of rational maps

$$\mathcal{I} = \frac{1}{4\pi} \int \left(\frac{1 + |z|^2}{1 + |R|^2} \left| \frac{dR}{dz} \right| \right)^4 \frac{2i dz d\bar{z}}{(1 + |z|^2)^2}. \quad (2.10)$$

The functional (2.10) is precisely the same quantity that appears in the rational map approximation of Skyrmions [3], and in both situations this is the only contribution to the energy that distinguishes between rational maps of the same degree N . This proves that, within the rational map approximation, the minimal energy monopole of charge N in AdS has the same rotational symmetries as the minimal energy Skyrmion with baryon number N and massless pions in Minkowski spacetime.

Previous results on rational maps, obtained in the context of Skyrmions, will therefore be of use later in this paper. For example, an inequality that follows simply from (2.8) and (2.10) is $\mathcal{I} \geq N^2$ [3]. Furthermore, for a large range of N , including all $N \leq 40$, the rational maps that minimize \mathcal{I} have been computed numerically [3, 15, 16], and their symmetries identified. Recall that a rational map is symmetric under a group $G \in SO(3)$ if a spatial rotation $g \in G$, which acts on the Riemann sphere coordinate z as an $SU(2)$ Möbius transformation, can be compensated by an $SU(2)$ Möbius transformation acting on the target Riemann sphere coordinate R . A rotation on the target sphere corresponds to a gauge transformation, and hence a symmetry, of the monopole.

The monopole fields (2.6) are consistent with the static field equations only if the rational map is spherically symmetric. The only spherically symmetric rational map is the (unique up to the action of $SU(2)$ Möbius transformations) degree one map $R = z$. In this case $\mathcal{I} = N = 1$ and the rational map approximation is exact, with the expression (2.9) for E^{rat} reproducing the true monopole energy. In this case the ordinary differential equations for the profile functions H and K , that follow from the variation of (2.9), agree with those appearing in the previous investigations [10, 11] of the single monopole in AdS.

A numerical construction of the profile functions allows a computation of the 1-monopole energy as a function of the AdS radius L . The results reveal that for $L \gtrsim \frac{1}{3}$ the energy is well-approximated by the formula $E \approx 2\pi(1 + \frac{2}{5}L^{-1})$. In particular, the energy is $E = 2\pi \times 1.396$ for $L = 1$. In all the numerical computations presented in this paper the value $L = 1$ will be chosen as a generic radius. The above result shows that for this radius the energy of the single monopole is increased by around 40% from the flat space limit, which should be sufficient to observe the phenomena that arise due to the curvature of AdS. In the analytic approximations the dependence on L will be retained, allowing the qualitative behaviour with L to be deduced.

For each charge N , using the minimal value of \mathcal{I} in (2.9) and numerically computing the profile functions H and K , produces an energy E^{rat} which is an upper bound on the true

minimal energy of the N -monopole. The energies E^{rat} (in units of 2π) are plotted as the circles in Figure 1 for $1 \leq N \leq 17$.

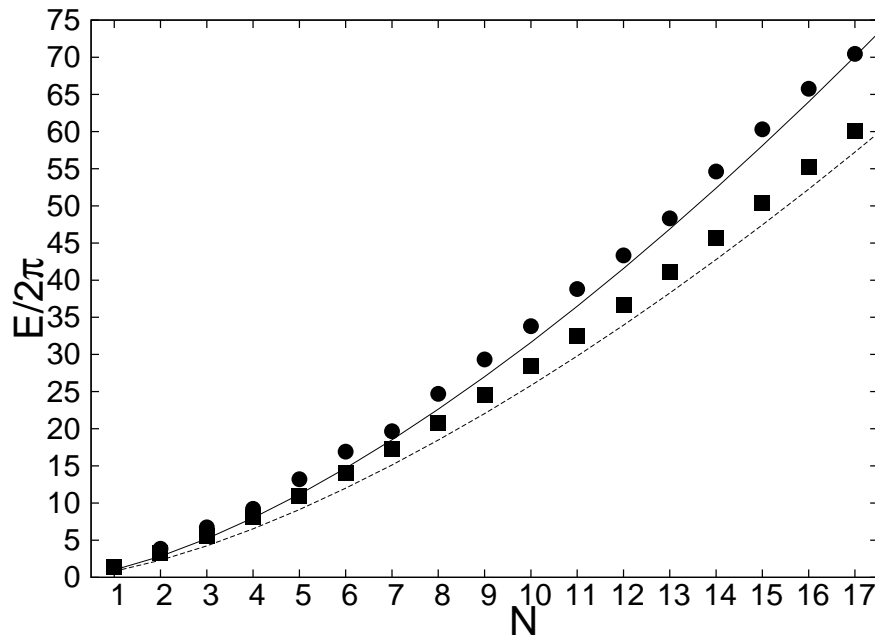


Figure 1: The energy (in units of 2π) for monopoles with charge $N \leq 17$. Circles denote the values obtained from the rational map approximation and squares are the results of field theory simulations. The solid curve is $N^{3/2}$ and the dashed curve is the magnetic bag approximation.

The rational map approximation may be related to the magnetic bag approximation [7, 1] by making a series of further simplifications, as described below. The magnetic bag approximation assumes that the fields take different forms inside and outside a bag of radius $\rho = \sigma$. Inside the bag, that is $\rho \in [0, \sigma)$ the profile functions are taken to be $H = 0$ and $K = 1$, so that the energy density vanishes. For $\rho > \sigma$, which is the outside of the bag, the magnetic field is taken to be abelian by setting $K = 0$. With these simplifications the energy E^{rat} becomes

$$E_{bag}^{rat} = 4\pi L \int_{\sigma}^1 \left\{ \frac{\rho^2 H'^2}{(1 - \rho^2)^2} + \frac{\mathcal{I}}{16L^2 \rho^2} \right\} (1 + \rho^2) d\rho, \quad (2.11)$$

where the contribution from the surface of the bag has been ignored, which means that E_{bag}^{rat} is no longer guaranteed to be an upper bound for the true monopole energy. The boundary condition on the surface of the bag is $H(\sigma) = 0$, and the energy minimizing profile function is easily found to be

$$H = \frac{h(\sigma) - h(\rho)}{h(\sigma) - \pi}, \quad (2.12)$$

where the function

$$h(\rho) = \frac{1}{\rho} - \rho + 4 \tan^{-1} \rho, \quad (2.13)$$

has been introduced. The resulting energy depends on the bag radius σ via

$$E_{bag}^{rat} = 4\pi \left\{ \frac{L}{h(\sigma) - \pi} + \frac{\mathcal{I}}{16L\sigma} (1 - \sigma^2) \right\}. \quad (2.14)$$

The magnetic bag approximation is expected to be accurate for large charge $N \gg L$, when the bag radius approaches the AdS boundary, that is, $\sigma = 1 - \varepsilon$ with $0 < \varepsilon \ll 1$. To leading order in ε

$$E_{bag}^{rat} = 2\pi \left(\frac{3L}{\varepsilon^3} + \frac{\mathcal{I}\varepsilon}{4L} \right), \quad (2.15)$$

and the energy is minimized when $\varepsilon = \sqrt{6L}/\mathcal{I}^{1/4}$, to give the value

$$E_{bag}^{rat} = 2\pi \sqrt{\frac{2}{3L}} \mathcal{I}^{3/4} \approx 2\pi \sqrt{\frac{N^3}{L}} \quad (2.16)$$

where the final approximation uses the fact that, for a large range of N , numerical results reveal [16] that $\mathcal{I} \approx 1.3N^2 \approx (\frac{3}{2})^{2/3} N^2$. In fact, the analysis in section 4 suggests the limiting behaviour $\mathcal{I}/N^2 \rightarrow 1.21$ as $N \rightarrow \infty$, which is consistent with the numerical results for large N .

The solid curve in Figure 1 is the function $N^{3/2}$, obtained from the approximation (2.16) by setting $L = 1$. It can be seen that this approximation is a reasonable fit to the numerical data (circles) and confirms the superlinear growth of E^{rat} with N . As discussed in the introduction, in AdS a superlinear growth of the monopole energy with charge does not imply that the N -monopole is unstable to fragmentation into individual monopoles.

The original magnetic bag approximation [7, 1] assumes that the angular distribution is spherical. In terms of the rational map approximation this corresponds to the assumption that the winding density

$$\left(\frac{1 + |z|^2}{1 + |R|^2} \left| \frac{dR}{dz} \right| \right)^2, \quad (2.17)$$

appearing in the expression (2.8) for the charge, is constant. Of course, the only rational map for which this is true is the degree one map $R = z$, corresponding to the fact that there are no spherical monopoles with $N > 1$. However, ignoring this fact and assuming that the density (2.17) is constant, then it must be equal to N . In which case $\mathcal{I} = N^2$, so the spherical assumption is equivalent to approximating \mathcal{I} by its lower bound N^2 . With this additional simplification the energy E_{bag}^{rat} in (2.16) becomes the bag energy

$$E_{bag} = 2\pi \sqrt{\frac{2N^3}{3L}} \quad (2.18)$$

first obtained by Bolognesi and Tong [1]. The dashed curve in Figure 1 is this magnetic bag energy.

The energy E^{rat} of the rational map approximation is an upper bound for the true monopole energy, and the bag energy E_{bag} is obtained by neglecting certain contributions to the energy and assuming an idealized spherical distribution. It might therefore be expected that the true monopole energy lies between these two approximations. In the following section numerical results will be presented that confirm this expectation, using simulations of the full non-abelian nonlinear field theory.

3 Field theory simulations

To perform numerical field theory simulations it is convenient to introduce Cartesian type coordinates \mathbf{x} , defined inside the unit ball, so that the sausage metric becomes

$$ds^2 = -\left(\frac{1+\rho^2}{1-\rho^2}\right)^2 dt^2 + \frac{4L^2 d\mathbf{x} \cdot d\mathbf{x}}{(1-\rho^2)^2}, \quad (3.1)$$

where $\rho^2 = \mathbf{x} \cdot \mathbf{x} \leq 1$.

The numerical monopole solutions are obtained by performing a simulated annealing energy minimization algorithm on the associated static energy

$$E = \int -\frac{1}{2} \text{Tr} \left\{ \frac{1}{8L} F_{ij}^2 + \frac{L}{(1-\rho^2)^2} (D_i \Phi)^2 \right\} (1+\rho^2) d^3x. \quad (3.2)$$

The coordinates \mathbf{x} are discretized on a regular lattice with lattice spacing $dx = 0.02$, and the simulation grid contains all the points of the lattice that satisfy $\mathbf{x} \cdot \mathbf{x} \leq 1$. Spatial derivatives are approximated using a second order finite difference scheme and the energy is computed at points of the dual lattice. On the boundary of the grid the vacuum expectation value of the Higgs field is enforced $|\Phi| = 1$, and Φ is fixed at the sampled values of a continuum field with winding number N . Explicitly, on the boundary $\Phi = i\mathbf{n} \cdot \boldsymbol{\tau}$ with \mathbf{n} given in terms of a degree N rational map via (2.5). In theory, all degree N rational maps should provide equivalent boundary conditions, as the winding number of the Higgs field is the only gauge invariant quantity. However, on the lattice there is likely to be a small bias against rational maps with extreme angular derivatives.

The final ingredient required for the numerical simulation is an initial condition. The only requirement on the initial fields is that the Higgs field on the boundary must take the form described above, namely $\Phi = i\mathbf{n} \cdot \boldsymbol{\tau}$, with \mathbf{n} determined by a particular rational map. The simplest possibility is to take the initial fields to be

$$\Phi = i\rho\mathbf{n} \cdot \boldsymbol{\tau}, \quad A_j = 0. \quad (3.3)$$

Note that in the continuum theory this initial field does not have finite energy, because $D_j \Phi$ does not vanish on the boundary. However, this is not a problem on the lattice, and the gauge potential evolves during the simulation, and in particular at the boundary, to drive $D_j \Phi$ towards zero at the boundary. A more sophisticated initial condition could be used,

N	G	$E/(2\pi)$
1	$O(3)$	1.39
2	$D_{\infty h}$	3.29
3	T_d	5.54
4	O_h	8.08
5	D_{2d}	10.94
6	D_{4d}	14.01
7	Y_h	17.29
8	D_{6d}	20.83
9	D_{4d}	24.55
10	D_{4d}	28.41
11	D_{3h}	32.49
12	T_d	36.71
13	O	41.08
14	D_2	45.65
15	T	50.33
16	D_3	55.29
17	Y_h	60.07

Table 1: The symmetry group and energy (in units of 2π) for monopoles with charge $N \leq 17$.

for example by starting with the fields of the rational map approximation, but this is not necessary.

An indication of the numerical accuracy of the algorithm can be obtained by computing the charge N , of the final configuration, using the lattice version of (2.3). For the results presented in this section the numerical charge is integer-valued to an accuracy of within 0.1% for $N \leq 4$, with the error rising to 1% for $N = 17$, which is the largest value considered.

The minimal energies obtained from field theory simulations are presented in Table 1 and plotted as the squares in Figure 1. As expected, these energies lie between the values predicted by the rational map and magnetic bag approximations. The rational map approximation is more accurate for small values of N , but the magnetic bag approximation becomes increasingly accurate as N increases.

To obtain these numerical results the rational map used in the initial (and boundary) condition is the \mathcal{I} minimizing map for each value of N . The symmetry of this map, which is also found to be the symmetry of the final numerical solution, is listed in Table 1. Energy density isosurfaces are displayed in Figure 2 for a selection of monopoles with continuous or Platonic symmetries. For $N > 2$ the energy density is localized on the edges, and particularly the vertices, of a polyhedron. For the larger charges shown in Figure 2 the pattern emerges of a polyhedron with $2N - 2$ faces, of which 12 are pentagons and the remainder are hexagons. Such polyhedra are familiar from the study of fullerenes in carbon chemistry, with the charge 17 monopole providing the most famous example of the truncated icosahedron, associated with the buckyball. The monopole energy density isosurfaces presented in Figure 2 are

qualitatively the same as those for Skyrmions, where the connection with fullerenes was first observed [15].

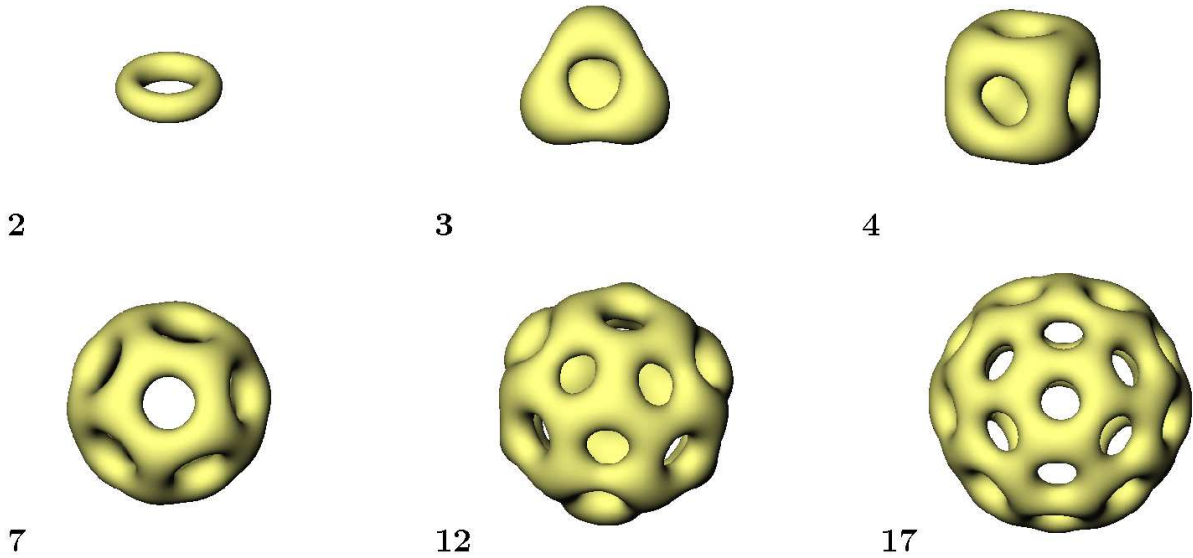


Figure 2: Energy density isosurfaces for monopoles with charges $N = 2, 3, 4, 7, 12, 17$. Each of these monopoles has either a continuous or Platonic symmetry and the plots are displayed to scale.

Note that the difference between the approximate rational map energy (the last expression in (2.16)) and the magnetic bag energy (2.18) is a factor $\sqrt{3/2} = 1.22\dots$. This suggests that generically the energy of the rational map approximation may be as much as 20% above the true value. This is much larger than the error in the rational map approximation to Skyrmions [3], which is typically a few percent. This means that some caution must be exercised when concluding that the symmetry predicted by the rational map approximation is indeed the symmetry of the minimal energy monopole. However, the fact that the numerical solutions, which share the same symmetries as the rational maps, have energies that tend towards the magnetic bag values, suggests that these solutions are strong candidates for minimal energy monopoles.

Further evidence to support this claim is provided by considering alternative rational maps. For example, if the axially symmetric degree three rational map $R = z^3$ is used to provide the initial (and boundary) conditions for the simulation then an axially symmetric 3-monopole is obtained with an energy $E = 2\pi \times 5.64$; this is a little larger than the energy $E = 2\pi \times 5.54$ of the tetrahedrally symmetric 3-monopole. Furthermore, symmetry breaking perturbations of axially symmetric maps have been simulated for $N = 3$ and $N = 4$ by using the rational map $R = z^N + \frac{1}{10}z^{N-1}$. In both cases the final numerical solution obtained is a Platonic monopole (tetrahedral for $N = 3$ and cubic for $N = 4$), making it extremely likely that these are the minimal energy monopoles. It is difficult to perform similar simulations

using asymmetric maps for larger values of N , both because of the dramatically increased simulation time required in comparison to symmetric maps, and the fact that the perturbed map must remain as the boundary map throughout the simulation, which leads to increased angular derivatives as the charge increases.

Other symmetric maps that are not \mathcal{I} minimizing have also been used in simulations. For example, there is a degree five map with octahedral symmetry [3] that yields a numerical solution for an octahedron with energy $E = 2\pi \times 10.98$; this is slightly larger than the energy $E = 2\pi \times 10.94$ of the less symmetric 5-monopole with only D_{2d} symmetry. There is also an icosahedrally symmetric degree eleven map [3] that produces an icosahedron with an energy $E = 2\pi \times 32.85$, again larger than the less symmetric D_{3h} 11-monopole with energy $E = 2\pi \times 32.49$. It seems likely that these additional solutions are saddle points.

The rational map approximation will predict the correct symmetry of the minimal energy monopole providing the error in the approximation is similar for competing local minima. One situation in which this is clearly not the case is the flat space limit $L \rightarrow \infty$ of Minkowski spacetime, with its $4N$ -dimensional BPS moduli space \mathcal{M}_N . The rational map approximation (2.6) survives the limit to Minkowski spacetime, but it does not capture the BPS moduli space. In this case, the rational map dependence of the energy is not a physical property but rather an indication of the failure of the rational map approximation to accurately describe a particular monopole in the moduli space. The rational map approximation is at its most accurate for shell-like configurations, hence \mathcal{I} may be thought of as a measure of the deviation from spherical symmetry of an N -monopole, which is unattainable for $N > 1$. For example, for $N = 4$ the \mathcal{I} minimizing map has cubic symmetry and the fields (2.6) provide an approximation to the exact cubic 4-monopole [4], which may be regarded as the point in \mathcal{M}_4 which is the closest to a spherical 4-monopole. In this example the energy of the rational map approximation turns out to be 10% above the BPS energy, and the error is obviously greater than this in attempting to describe any other monopole in the moduli space \mathcal{M}_4 . Despite these limitations, the rational map approximation may turn out to be useful in Minkowski spacetime, as it provides explicit monopole fields that can be used in analytic approximations, or to provide initial conditions in any numerical computations involving monopoles.

The magnetic bag approximation assumes that the Higgs field vanishes throughout a ball. However, exact monopole solutions have a finite number of zeros of the Higgs field. In the rational map approximation it is assumed that there is a single zero at the origin, with multiplicity N for an N -monopole. This is a correct description of almost all the numerical monopole solutions presented in this paper. The exceptions are the monopoles of charges three, five and eleven, describing a tetrahedron, octahedron and icosahedron respectively. For these monopoles, of which only the $N = 3$ example is minimal energy, the associated polyhedron has triangular faces and $N + 1$ vertices. There are $N + 1$ zeros of the Higgs field associated with these vertices (but at a smaller distance from the origin) plus an additional zero of the Higgs field at the origin with a negative multiplicity (termed an anti-zero). This mirrors the situation in Minkowski spacetime, where the same phenomenon has been discovered for the tetrahedral $N = 3$ and octahedral $N = 5$ examples [17, 18] using the

Nahm transform. The $N = 11$ icosahedral example has not been investigated in Minkowski spacetime because the Nahm data is not known in this case.

In Figure 3 the properties of the icosahedral 11-monopole in AdS are displayed. On the left is an energy density isosurface, confirming that the energy density is maximal on the vertices of an icosahedron. On the right is a plot to highlight the positions of the zeros of the Higgs field, by displaying an isosurface where $|\Phi|$ is small; in this particular case $|\Phi| = 0.06$. This plot reveals that there are 12 zeros of the Higgs field on the vertices of an icosahedron and an anti-zero at the origin. The surface around the anti-zero appears much larger than that around the 12 zeros, which may indicate that the variation of the length of the Higgs field is reduced around the anti-zero. However, this conclusion is not certain because of the visual distortion in size associated with the AdS metric.

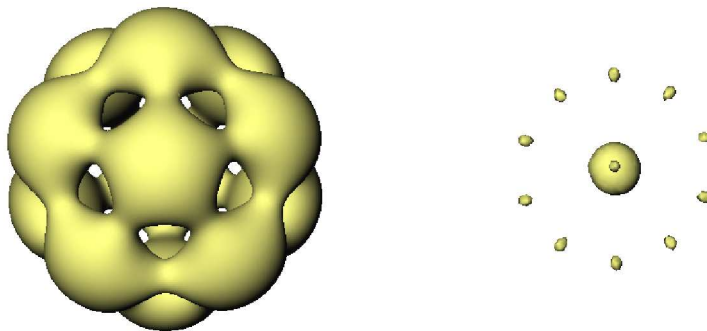


Figure 3: On the left is an energy density isosurface for the icosahedral 11-monopole. On the right (to scale) is the associated isosurface where $|\Phi| = 0.06$, indicating the positions of the zeros of the Higgs field. There are 12 zeros on the vertices of an icosahedron and an anti-zero at the origin.

It has been suggested, at least in Minkowski spacetime, that there may be different types of monopole bags depending upon whether the zeros of the Higgs field are located at the origin or on the shell of the bag [19]. The numerical results in AdS show that there are indeed two different types of monopole solutions characterized either by N zeros at the origin or $N + 1$ zeros near the points of maximal energy density, plus an anti-zero at the origin. In AdS it appears that for $N > 3$ the former type of monopole solution has lower energy.

4 Monopole walls

In the large N limit, monopoles in AdS can be studied by zooming to the Poincaré patch of AdS. This results in the emergence of a monopole wall, associated with the shell of the N -monopole on which the energy density is maximal. Monopole walls were initially studied by Ward [8] in Minkowski spacetime, as novel domain walls in which the magnetic field along a line perpendicular to the wall tends to zero on one side of the wall and to a non-zero constant on the other side of the wall. In contrast to standard domain walls, the fields are

not independent of the coordinates perpendicular to the wall, but are periodic with a spatial variation of the energy density and magnetic field.

In Minkowski spacetime monopole walls have infinite energy per unit area. However, in AdS the energy per unit area of a monopole wall is finite, and can be investigated using a magnetic bag style approximation [1]. The magnetic bag approximation ignores the spatial distribution of the fields within the wall, and is therefore unable to make any predictions about the symmetry or lattice structure of the wall. Numerical results in Minkowski spacetime [8] are unable to shed any light on this issue, as the symmetry is controlled by free parameters in the solution, that are essentially inherited from the BPS moduli space for finite charge.

A variant of the rational map approximation is introduced in this section, that is suitable for studying monopole walls in AdS. This approximation is refined enough to address the spatial distribution of the fields and suggests that the minimal energy per unit area is obtained from a monopole wall with a hexagonal lattice. Numerical simulations are performed that support this conclusion, which is again in agreement with the Skyrme model, where a similar hexagonal lattice exists [9].

In most applications of holographic methods, the Poincaré patch of AdS is the correct arena in which to apply the AdS/CFT correspondence. The results of an analysis of monopole walls in AdS is therefore likely to be of some interest within the context of holography, and in particular for applications to condensed matter systems where magnetic fields play a prominent role.

In the Poincaré patch the planar metric of AdS reads

$$ds^2 = \frac{r^2}{L^2}(-dt^2 + dx^2 + dy^2) + \frac{L^2}{r^2}dr^2, \quad (4.1)$$

where $r \geq 0$ is the radial variable in the bulk, with three-dimensional Minkowski spacetime obtained at the ultra-violet boundary $r \rightarrow \infty$.

Working in a fundamental torus, \mathbb{T}^2 , in the (x, y) plane, the static energy in the volume $\mathbb{T}^2 \times \mathbb{R}$ is given by

$$E = \int -\frac{1}{4}\text{Tr}\left\{\left(\frac{L}{r}\right)^4 F_{xy}^2 + F_{xr}^2 + F_{yr}^2 + \left(\frac{r}{L}\right)^2 (D_r\Phi)^2 + \left(\frac{L}{r}\right)^2 \left((D_x\Phi)^2 + (D_y\Phi)^2\right)\right\}\left(\frac{r}{L}\right)^2 d^3x. \quad (4.2)$$

The wall version of the rational map approximation has the same form as (2.6)

$$\Phi = iH\mathbf{n} \cdot \boldsymbol{\tau}, \quad A_j = \frac{i}{2}(1 - K)(\mathbf{n} \times \partial_j\mathbf{n}) \cdot \boldsymbol{\tau}, \quad (4.3)$$

where $H(r), K(r)$ are profile functions and \mathbf{n} is again related to a Riemann sphere coordinate R through (2.5). However, in this case $R(z)$ is a periodic function in \mathbb{T}^2 , where $z = x + iy$ is the complex coordinate in the plane.

The boundary conditions on the profile functions are again determined by regularity and finite energy to be $H(0) = 0$, $H(\infty) = 1$, $K(0) = 1$, $K(\infty) = 0$, where the vacuum expectation value $|\Phi| \rightarrow 1$ as $r \rightarrow \infty$ has been imposed.

The ansatz (4.3) implies that $A_r = 0$ and

$$F_{xy} = 2i(1 - K^2)J\mathbf{n} \cdot \boldsymbol{\tau}, \quad (4.4)$$

where

$$J = \frac{1}{(1 + |R|^2)^2} \left| \frac{dR}{dz} \right|^2. \quad (4.5)$$

The monopole charge in the fundamental torus is the degree of the map from the torus to the sphere and is given by

$$N = \frac{1}{\pi} \int_{\mathbb{T}^2} J \, dx dy. \quad (4.6)$$

Using the approximate fields (4.3) and performing the integration over \mathbb{T}^2 yields

$$E = \int_0^\infty \left\{ A \left(\frac{r}{L} \right)^2 \frac{1}{2} H'^2 + N\pi \left(K'^2 + \left(\frac{L}{r} \right)^2 4H^2 K^2 \right) + \frac{2\mathcal{I}\pi^2}{A} \left(\frac{L}{r} \right)^4 (1 - K^2)^2 \right\} \left(\frac{r}{L} \right)^2 dr, \quad (4.7)$$

where A is the area of the torus \mathbb{T}^2 and

$$\mathcal{I} = \frac{A}{\pi^2} \int_{\mathbb{T}^2} J^2 \, dx dy, \quad (4.8)$$

is a quantity that is independent of the area A .

As $r \rightarrow \infty$ the abelian magnetic field perpendicular to the wall is

$$B = -\frac{1}{2} \text{Tr}(F_{xy} \Phi) = 2J, \quad (4.9)$$

with magnetic flux per unit area

$$B_\star = \frac{1}{A} \int_{\mathbb{T}^2} 2J \, dx dy = \frac{2\pi N}{A}. \quad (4.10)$$

There is a one-parameter family of magnetic walls, labelled by B_\star , the magnetic flux per unit area at the ultra-violet boundary. Using (4.7) and the definition (4.10) the energy per unit area of the wall may be written as

$$\frac{E}{A} = \int_0^\infty \left\{ \left(\frac{r}{L} \right)^2 \frac{1}{2} H'^2 + \frac{B_\star}{2} \left(K'^2 + \left(\frac{L}{r} \right)^2 4H^2 K^2 \right) + \frac{B_\star^2 \mathcal{I}}{2N^2} \left(\frac{L}{r} \right)^4 (1 - K^2)^2 \right\} \left(\frac{r}{L} \right)^2 dr. \quad (4.11)$$

Before presenting an analysis of the energy (4.11) it is first worth discussing the wall analogue of the magnetic bag approximation [1].

To the infra-red side of the wall $r < \sigma$, the profile functions are taken to be $H = 0$ and $K = 1$, so that the energy density vanishes. To the ultra-violet side of the wall $r > \sigma$, the simplification is to assume that $K = 0$, so that the energy per unit area becomes

$$\frac{E}{A} = \int_\sigma^\infty \left\{ \left(\frac{r}{L} \right)^2 \frac{1}{2} H'^2 + \frac{B_\star^2 \mathcal{I}}{2N^2} \left(\frac{L}{r} \right)^4 \right\} \left(\frac{r}{L} \right)^2 dr, \quad (4.12)$$

where once again the contribution on the wall $r = \sigma$ has been ignored.

The energy minimizing profile function, satisfying the boundary condition $H(\sigma) = 0$, is easily found to be

$$H = 1 - \frac{\sigma^3}{r^3}. \quad (4.13)$$

The position of the wall is

$$\sigma = \sqrt{\frac{B_\star L^3 \sqrt{\mathcal{I}}}{3N}} \quad (4.14)$$

with a resulting energy per unit area

$$\frac{E}{A} = \sqrt{\frac{4B_\star^3 L \mathcal{I}^{3/2}}{3N^3}}. \quad (4.15)$$

The final approximation required to reproduce the result of Bolognesi and Tong [1] is to assume that the magnetic field is independent of the coordinates parallel to the wall. This simplification implies that $B = B_\star = 2J$ is a constant, and hence the approximation $\mathcal{I} = N^2$. This yields the wall position and energy per unit area as

$$\sigma = \sqrt{\frac{B_\star L^3}{3}}, \quad \frac{E}{A} = \sqrt{\frac{4B_\star^3 L}{3}}. \quad (4.16)$$

Returning to the energy (4.11), an explicit expression for $R(z)$, the map from the torus to the sphere, is required to make further progress. To obtain a wall with hexagonal symmetry this map is chosen to be proportional to the Weierstrass elliptic function $\wp(z)$ defined by the equation

$$\wp'^2 = 4\wp^3 - 4. \quad (4.17)$$

This elliptic function has periods $\omega_1 = \Gamma(\frac{1}{6})\Gamma(\frac{1}{3})/(2\sqrt{3}\pi)$ and $\omega_2 = \omega_1 e^{i\pi/3}$, giving the required 60° angle between the fundamental periods. The precise form taken for the map is $R(z) = c\wp(z/a)$, where a and c are real constants, with a determined in terms of the area A of the torus by $a^2 = 2A/(\sqrt{3}\omega_1^2)$. Recall that \mathcal{I}/N^2 is independent of A (and hence a).

The elliptic function has a double pole in its fundamental parallelogram and describes a map with degree $N = 2$. Integrating over the torus reveals that \mathcal{I}/N^2 is minimized for $c = 0.70$, when it takes the value $\mathcal{I}/N^2 = 1.21$. Note that this value is consistent with the large N limit of the minimizing rational maps discussed earlier.

Using the value $\mathcal{I}/N^2 = 1.21$ allows the energy per unit area (4.11) of the elliptic map approximation to be calculated as a function of B_\star , by computing the minimizing profile functions. This energy is plotted as the solid curve in Figure 4 and provides an upper bound on the energy per unit area of the wall. The dashed curve is the energy (4.16) of the magnetic bag style approximation.

Numerical field theory simulations allow a computation of the monopole wall energy (4.2) using a simulated annealing algorithm similar to that discussed in the previous section. It is convenient to perform the simulations over two copies of the torus, so that a rectangular

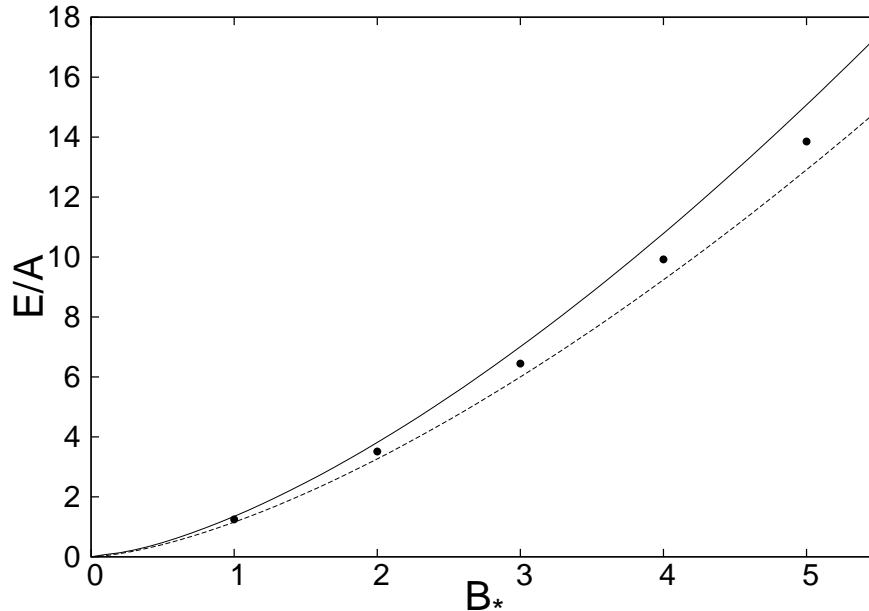


Figure 4: The energy per unit area E/A of the monopole wall as a function of B_* , the magnetic flux per unit area at the ultra-violet boundary. The solid curve is the hexagonal elliptic map approximation, the dashed curve is the magnetic bag style approximation and the circles are the results from field theory simulations.

domain $(x, y) \in [0, a\omega_1] \times [0, \sqrt{3}a\omega_1]$ may be used with periodic boundary conditions. The numerical grid contained 52×90 grid points to cover each rectangle.

It is numerically more efficient if all the spatial coordinates take values in a finite range, hence the simulations use the variable $u = r/(1+r)$, taking values in the unit interval. This interval is covered with 50 grid points, so the total grid contains $52 \times 90 \times 50$ points. The initial conditions are taken from the elliptic map approximation.

The results of the numerical simulations are displayed as the circles in Figure 4, which lie between the elliptic map approximation and the magnetic bag style approximation. As in the case of monopoles in global AdS, this suggests that the magnetic bag style approximation may provide a lower bound on the energy, to complement the upper bound of the elliptic map approximation.

In Figure 5 the image on the left is an energy density isosurface for the numerical solution with $B_* = 10$, where the hexagonal structure of the lattice is clearly visible. As the region contains two copies of the torus then the charge in the displayed region is $N = 4$.

In Figure 6 the length of the Higgs field $|\Phi|$ is plotted as a function of $r/(1+r)$ for the case $B_* = 1$. The dashed curve is the elliptic map approximation and the dotted curve is the magnetic bag style approximation. The solid curve is the result from field theory simulations, plotted along a generic line perpendicular to the wall. It can be seen that the elliptic map approximation is in excellent agreement with the field theory simulations, and

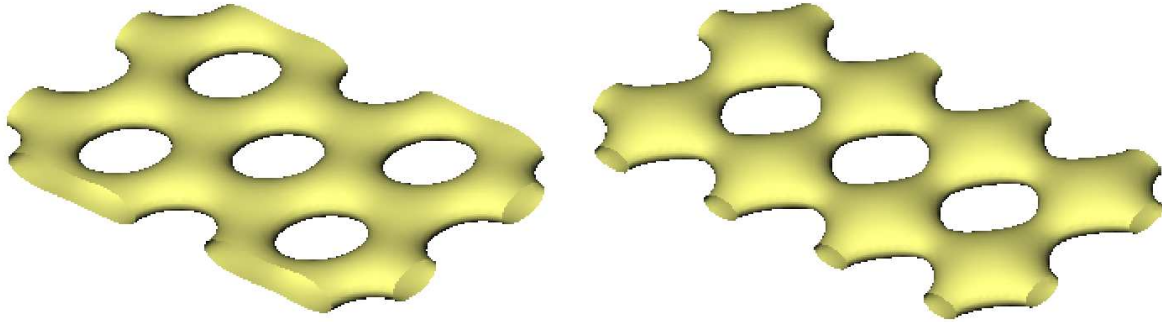


Figure 5: Energy density isosurfaces for monopole walls with $B_\star = 10$. On the left is the hexagonal wall and on the right is the square wall, which has a slightly higher energy.

the magnetic bag approximation provides a good description everywhere except around the actual wall itself.

A monopole wall with a square lattice can be obtained by using the Weierstrass elliptic function $\tilde{\wp}(z)$ defined by the equation

$$\tilde{\wp}'^2 = 4\tilde{\wp}^3 - 4\tilde{\wp}, \quad (4.18)$$

which has periods $\tilde{\omega}_1 = \Gamma(\frac{1}{4})^2/(2\sqrt{2\pi})$ and $\tilde{\omega}_2 = i\tilde{\omega}_1$, producing a 90° angle between the fundamental periods.

Taking a map of the form $R(z) = \tilde{c}\tilde{\wp}(z/\tilde{a})$, with $\tilde{a}^2 = A/\tilde{\omega}_1^2$, reveals that \mathcal{I}/N^2 is minimized for $\tilde{c} = 1.00$, when it takes the value $\mathcal{I}/N^2 = 1.30$. This is greater than that of the hexagonal lattice, and supports the view that a hexagonal architecture produces minimal energy.

Further evidence is provided by using the approximate fields of the square wall as initial conditions in the field theory simulations. To facilitate a comparison with the simulations of the hexagonal wall, two copies of the torus are again taken, by using the rectangular domain $(x, y) \in [0, \tilde{a}\tilde{\omega}_1] \times [0, 2\tilde{a}\tilde{\omega}_1]$, covered by 50×100 grid points. In Figure 5 the image on the right is an energy density isosurface for the resulting numerical solution with $B_\star = 10$. The energy per unit area of this square wall is $E/A = 39.5$, which is slightly greater than the value $E/A = 39.1$ for the corresponding hexagonal wall. For comparison, the energy per unit area of the magnetic bag style approximation is $E/A = 36.5$.

5 Conclusion

Motivated by applications in holographic theories, a detailed analytic and numerical study has been performed for monopoles in AdS, and the associated monopole walls that arise in the large charge limit. An approximation has been introduced, using rational maps between Riemann spheres, and it has been confirmed that this provides a reasonable description of

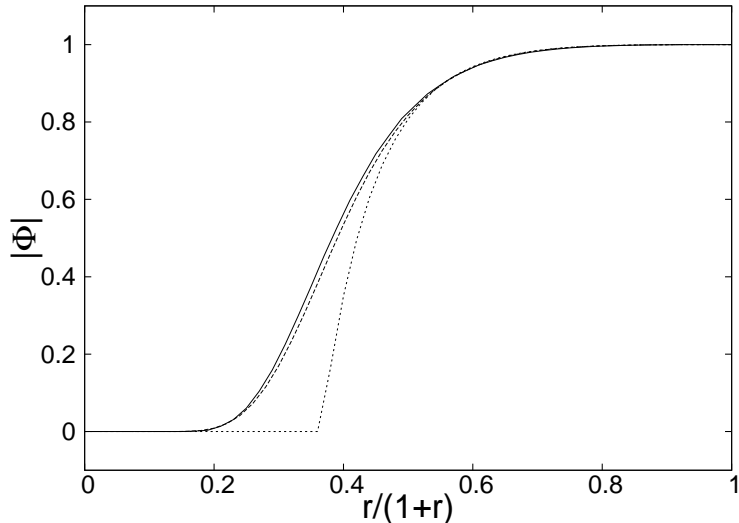


Figure 6: $|\Phi|$ as a function of $r/(1+r)$. The dashed curve is the elliptic map approximation, the dotted curve is the magnetic bag style approximation, and the solid curve is the result from field theory simulations.

the fields when compared with the results from field theory simulations. The results of these simulations also confirm that the magnetic bag approximation yields energies that are close to the true monopole energies, even for reasonably small values of the charge.

The arguments presented in [1] suggest that, for certain regions of parameter space, the monopole wall (with its lattice structure) may be favoured over the more conventional magnetically charged black hole, which is homogeneous at the ultra-violet boundary. It would be interesting to investigate this issue by extending the methods described in this paper, for a fixed AdS background, to the situation including gravitational backreaction and finite temperature.

Finally, the connection between monopoles and Skyrmions in Minkowski spacetime has been enhanced by considering monopoles in AdS. A natural extension would therefore be to study Skyrmions in AdS, to make a comparison with the results presented here for monopoles. The rational map approximation easily extends to Skyrmions in AdS and yields the same functional on the space of rational maps. This would seem to imply that monopoles and Skyrmions in AdS have a similar form. However, there is a caveat to this conclusion. It appears that, as far as Skyrmions are concerned, the curvature of hyperbolic space plays a similar role to that of a pion mass [20]. It is known that Skyrmions with massive pions, in Minkowski spacetime, are shell-like (and hence described by the rational map approximation) only for sufficiently low baryon numbers, and take a different form, including clusters, above a critical value [21, 22]. It may therefore be possible that Skyrmions in AdS could take more exotic forms than monopoles, such as clusters or multiple shells. It might be interesting to explore these possibilities.

Acknowledgements

Many thanks to Gary Gibbons, Ruth Gregory, Derek Harland, Mukund Rangamani, Simon Ross, David Tong, Claude Warnick and Marija Zamaklar for useful discussions.
I acknowledge STFC and EPSRC for grant support.

References

- [1] S. Bolognesi and D. Tong, *JHEP* **1101**, 153 (2011).
- [2] N. S. Manton and P. M. Sutcliffe, *Topological Solitons*, Cambridge University Press (2004).
- [3] C. J. Houghton, N. S. Manton and P. M. Sutcliffe, *Nucl. Phys.* **B510**, 507 (1998).
- [4] N. J. Hitchin, N. S. Manton and M. K. Murray, *Nonlinearity* **8**, 661 (1995).
- [5] C. J. Houghton and P. M. Sutcliffe, *Nonlinearity* **9**, 385 (1996).
- [6] W. Nahm, The construction of all self-dual multimonopoles by the ADHM method, in *Monopoles in Quantum Field Theory*, eds. N. S. Craigie, P. Goddard and W. Nahm, Singapore, World Scientific, 1982.
- [7] S. Bolognesi, *Nucl. Phys.* **B752**, 93 (2006).
- [8] R. S. Ward, *Phys. Rev.* **D75**, 021701 (2007).
- [9] R. A. Battye and P. M. Sutcliffe, *Phys. Lett.* **B416**, 385 (1998).
- [10] A. R. Lugo and F. A. Schaposnik, *Phys. Lett.* **B467**, 43 (1999).
- [11] A. R. Lugo, E. F. Moreno and F. A. Schaposnik, *Phys. Lett.* **B473**, 35 (2000).
- [12] E. Radu and D. H. Tchrakian, *Phys. Rev.* **D71**, 064002 (2005).
- [13] M. F. Atiyah, Magnetic monopoles in hyperbolic spaces, in *M. Atiyah: Collected Works, vol. 5*, Oxford, Clarendon Press, 1988.
- [14] S. Jarvis, *J. reine angew. Math.* **524**, 17 (2000).
- [15] R. A. Battye and P. M. Sutcliffe, *Phys. Rev. Lett.* **86**, 3989 (2001); *Rev. Math. Phys.* **14**, 29 (2002).
- [16] R. A. Battye, C. J. Houghton and P. M. Sutcliffe, *J. Math. Phys.* **44**, 3543 (2003).
- [17] C. J. Houghton and P. M. Sutcliffe, *Nucl. Phys.* **B464**, 59 (1996).
- [18] P. M. Sutcliffe, *Phys. Lett.* **B376**, 103 (1996).

- [19] K. Lee and E. J. Weinberg, *Phys. Rev.* **D79**, 025013 (2009).
- [20] M. F. Atiyah and P. M. Sutcliffe, *Phys. Lett.* **B605**, 106 (2005).
- [21] R. A. Battye and P. M. Sutcliffe, *Phys. Rev.* **C73**, 055205 (2006).
- [22] R. A. Battye, N. S. Manton and P. M. Sutcliffe, *Proc. R. Soc. Lond.* **A463**, 261 (2007).